JOURNAL OF AIRCRAFT
Vol. 40, No. 3, May–June 2003

Effect of Leading-Edge Curvature on Airfoil Separation Control

D. Greenblatt* and I. Wygnanski†
Tel Aviv University, 69978 Ramat Aviv, Israel

Separation control on NACA 0012 and NACA 0015 airfoils was compared under incompressible conditions, using leading-edge periodic excitation, in order to assess the effect of leading-edge curvature. Both lift and moment coefficients were considered to compare and analyse control effectiveness. In contrast to the relatively mild NACA 0015 trailing-edge stall, NACA 0012 stall was dominated by a leading-edge bubble-bursting mechanism that gave rise to alternating intervals of partial attachment and separation, but with no regular frequency. Low-amplitude excitation downstream of the bubble enhanced poststall lift and significantly attenuated the associated unsteadiness. In general, larger momentum coefficients were required for NACA 0012 separation control due to the large centrifugal acceleration of the flow around the leading edge. Because of the different stalling characteristics, relatively high- and low-excitation frequencies were effective for the NACA 0012 and NACA 0015 airfoils, respectively. However, the combination of high-excitation amplitudes with relatively low frequencies was effective on the NACA 0012, and this was believed to be associated with the large harmonic content of the evolving perturbations.

Nomenclature

C_d	=	drag coefficient, d/cq
C_l	=	lift coefficient, l/cq
$C_{l,\max}$	=	maximum lift coefficient
C_m	=	quarter-chord pitching moment coefficient, m/c^2q
C_P	=	pressure coefficient, $(p - p_\infty)/q$
C_μ	=	steady momentum coefficient, J/cq; oscillatory momentum coefficient, $\langle J \rangle/cq$
c	=	airfoil chord
F^+	=	reduced excitation frequency, $f_e X_{\text{te}}/U$
f	=	frequency
f_e	=	excitation frequency
f^+	=	reduced frequency, $f X_{\text{te}}/U$
h	=	slot width
J	=	steady jet momentum, $\rho U_J^2 h$
$\langle J \rangle$	=	oscillatory jet momentum, $\rho u_J^2 h$
p	=	local pressure
q	=	freestream dynamic pressure, $\rho U^2/2$
R	=	leading-edge radius of curvature
Re	=	chord Reynolds number, $\rho U c/\mu$
T	=	dimensionless time, tU/c
t	=	time
U	=	freestream velocity
U_e	=	local freestream velocity
U_J	=	mean component of slot velocity
u_J	=	oscillatory component of slot velocity
X_{te}	=	distance from slot location to trailing edge
x/c	=	normalized chordwise distance
α	=	incidence angle
α_s	=	static-stall angle
μ	=	air dynamic viscosity
ρ	=	air density
$'$	=	rms quantity

Received 21 May 2002; revision received 15 December 2002; accepted for publication 17 December 2002.

*Postdoctoral Fellow, Department of Fluid Mechanics and Heat Transfer; currently NRC Associate, Flow Physics and Control Branch, NASA Langley Research Center, Mail Stop 170, 1 East Reid Street, Hampton, VA, 23681-2199. Senior Member AIAA.

†Lazarus Professor of Aerodynamics, Department of Fluid Mechanics and Heat Transfer, also Professor of Aerospace Engineering, University of Arizona, Tucson 85721. Fellow AIAA.

Introduction

DURING recent decades, separation control by hydrodynamic excitation (periodic addition of momentum) has been shown to be effective for improving airfoil performance as well as overall efficiency.[1] Separation control by this method has been demonstrated on a wide variety of airfoil types, but a disproportionately large emphasis has been placed on NACA 0015 airfoil studies, involving leading-edge and flap-shoulder excitation,[2] effects of sweep,[3] Reynolds number,[4] Mach number,[5] high-turbulence levels,[6] and dynamic pitching.[7] Although the NACA 0015 (hereafter 0015) is still used on a variety of aircraft, the NACA 0012 (hereafter 0012) enjoys far wider general application, particularly on rotorcraft blades and for control surfaces. This is due to near-ideal behavior of the center of pressure with varying incidence below stall ($\alpha < \alpha_s$), together with an extensive database for a wide range of conditions.[8]

Recently, poststall separation control on the 0012 at low Reynolds numbers was demonstrated by local surface vibrations near the leading edge at $F^+ \approx 2$ (Ref. 9). Control on a dynamically pitching 0012 has also been shown using discrete pulsed vortex-generator jets.[10] However, no systematic separation control study, employing of calibrated excitation frequencies and amplitudes, has been reported for the 0012. Extrapolating separation control results from the 0015 is unwise because the airfoils have inherently different stalling characteristics, with so-called trailing-edge stall characterizing the 0015 and leading-edge stall apparent on the 0012 (Ref. 11, 12). The different stalling characteristics are manifested primarily as a result of the difference in leading-edge radius, namely $R/c = 1.58\%$ (0012) and 2.48% (0015).

This paper summarizes the data from an investigation of static incompressible separation control on the 0012 and compares them with 0015 data (c.f., Ref. 13). Time-averaged as well as time-dependent aspects of separation and its control were considered for both airfoils (c.f., Ref. 14). The differences between 0012 and 0015 stall were initially assessed, and the impact of these differences on separation control was evaluated. Due consideration was given to the determination of effective excitation frequencies, as well as appropriate parameters for assessing control effectiveness. Much of this paper was structured with a rotorcraft bias; thus, lift enhancement and moment stall alleviation were predominantly used as the leading indicators of airfoil performance. Although most modern commercial and military flight vehicles employ custom-designed wing sections, the 0012 and 0015 represent two distinct paradigms of stall and its control. Thus, data acquired on this basis may be considered as an initial effort toward establishing design rules for control applications based on geometric or aerodynamic characteristics.

Airfoils and Experimental Setup

The 0012 airfoil model was constructed from aluminum with an 8-in. chord and a 24-in. span (610 × 203 mm). It was equipped with 50 surface pressure ports and a two-dimensional leading-edge slot (Fig. 1a). The airfoil was supported internally by aluminum ribbing that rendered an effectively hollow interior, which served as a plenum chamber. The slot was located at 5% chord, orientated at 45 deg to the chord line with a width $h = 0.6$ mm (Fig. 1a). When not used for excitation, the slot was smoothly taped closed. (The airfoil was further equipped with an additional leading-edge slot on the lower surface, as well an aft slot at 73% chord,[13] but these were not employed in the present investigation.) Surface pressure data were augmented by hot-wire measurements in the upper surface boundary layer, and surface-mounted tufts were used for rudimentary flow visualization.

Figure 1b shows the leading-edge detail of the 0015, which has been fully described previously.[2] Note that the slot is located at the leading edge ($x/c = 0$) and effectively forms a wall jet tangent to the airfoil leading edge. This is slot introduces a small discontinuity at the leading edge, $h/R = 5.5\%$ (slot width in Fig. 1b exaggerated for clarity), whereas the 0012 slot does not. Roughness strips (grit number 100), used to trip the boundary layer, were fixed to the leading edges of both airfoils and extended to 4% chord on both top and bottom surfaces.

The airfoils were mounted in the Meadow–Knapp low-speed, closed-loop wind tunnel (see Ref. 2), and incidence angle variation was achieved using a modification to the drive system described by Piziali.[15] Zero net mass-flux excitation, via a particular slot, was achieved by means of a rotating valve and a small centrifugal blower connected to the airfoils' plenum chamber. (See Bachar[16] for full details.) Both slots were calibrated across their span and width by hot-wire anemometry. Dynamic surface pressure measurements at all ports were made simultaneously using the PS4000 array of pressure transducers (AA Lab Systems, Ltd). Total drag measurements were made using a rake of total head probes at approximately four chord lengths downstream of the trailing edges.

Specific excitation frequencies were selected on the basis of their ability to 1) generate a peak velocity on the order of the freestream velocity and 2) attain a C_μ corresponding to the excitation frequency that was at least one order of magnitude larger than the higher harmonics. The uncertainty associated with the slot calibration was $\Delta C_\mu / C_\mu \leq 20\%$. To maximize the reduced frequency and amplitude ranges attainable by the excitation device,[16] the majority of airfoil testing was performed at, or above, $Re = 2 \times 10^5$, which is considered the minimum for meaningful aerodynamic data.[17] Reynolds number effects were checked, however, by conducting 0012 and 0015 experiments at $Re = 4.8 \times 10^5$ and 9×10^5 respectively. Previous experience has shown that control authority is not degraded at higher Reynolds numbers ($Re > 10^6$) providing that F^+ and C_μ are maintained.[4,18] In addition, control effectiveness was found to be virtually insensitive to the presence or absence of boundary-layer tripping. The maximum uncertainty associated with prestall aerodynamic coefficients was $\Delta C_l = \pm 0.01$, $\Delta C_m = \pm 0.002$, and $\Delta C_d = \pm 0.001$ respectively. Poststall uncertainty bounds are indicated on the relevant figures.

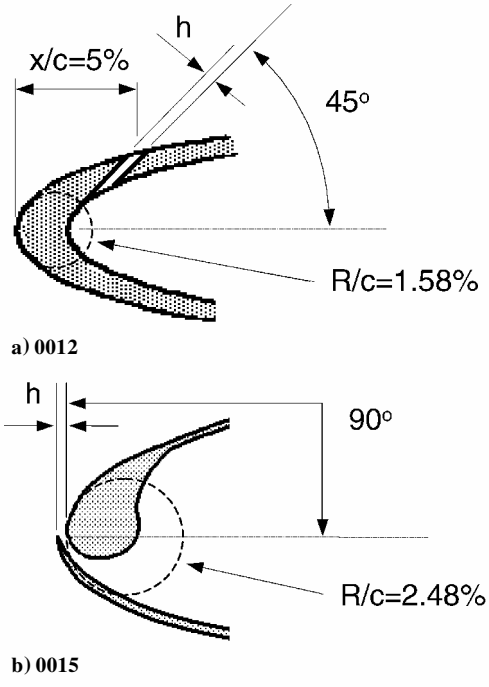

Fig. 1 Schematics of the 0012 and 0015 airfoils' leading-edge detail; 0015 slot width exaggerated for clarity.

Static-Stall Comparison

Static baseline (no control) 0012 lift and drag data were compared with those compiled by McCroskey[8] as well as with the high Reynolds number "standard roughness" data of Abbott and von Doenhoff[19] (not shown, see Ref. 13). $C_{l,\max}$ and C_{d0} were appropriate to the Reynolds number range tested presently (c.f., Ref. 8) and only minor discrepancies were observed between low and high Reynolds number data ($Re \leq 0.48 \times 10^6$ used presently vs $Re = 6 \times 10^6$ in Ref. 19). Furthermore, fully turbulent spectra in the upper surface boundary layer, $x/c = 30\%$ and $y/c = 0.5\%$, confirmed the effectiveness of the leading-edge roughness in tripping the flow (see Ref. 13).

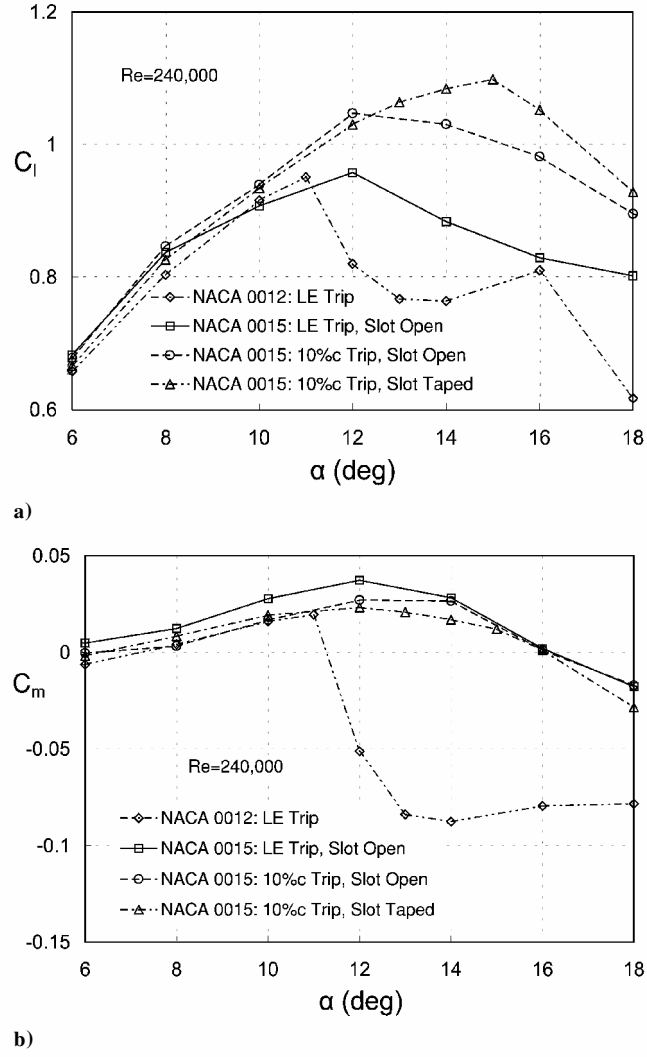

Fig. 2 Stalling characteristics of a) the NACA 0012 airfoil and b) the NACA 0015 airfoil.

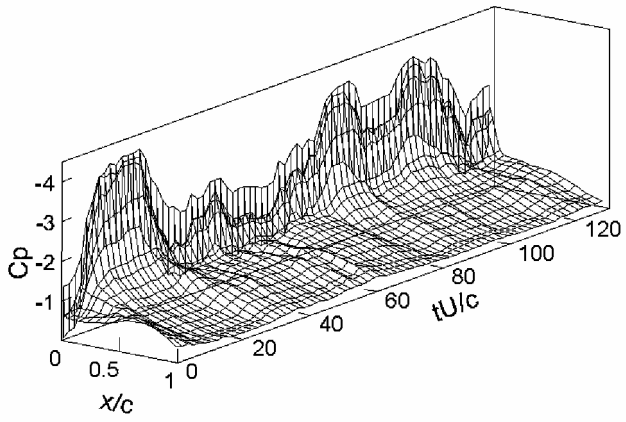

Fig. 3a Poststall upper-surface instantaneous pressure on the NACA 0012 airfoil $\alpha = \alpha_s + 1$ deg, $Re = 2.4 \times 10^5$.

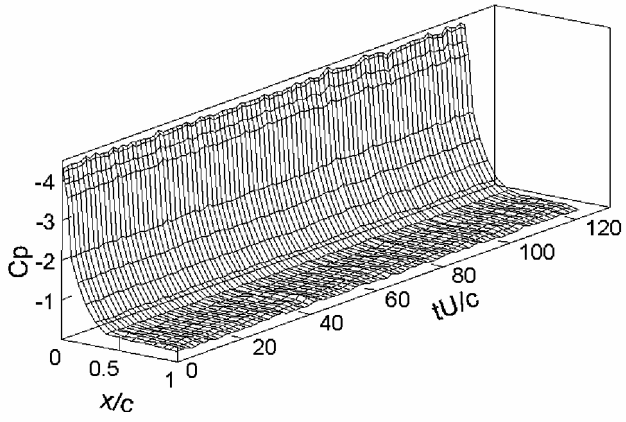

Fig. 3b Poststall up-surface instantaneous pressure on the NACA 0015 airfoil $\alpha = \alpha_s + 2$ deg, $Re = 2.4 \times 10^5$.

The essential difference between 0012 and 0015 static stall is shown in Figs. 2a and 2b. With both airfoil boundary layers tripped at the leading edge, the 0012 stalls sharply, $\alpha_s = 11$ deg, whereas the 0015 stalls gently, $\alpha_s = 12$ deg. Notwithstanding facility dependencies, these stalling characteristics are similar to those exhibited at high Reynolds numbers ($1.2 \times 10^6 \leq Re \leq 9 \times 10^6$) for both the 0012 (Refs. 19 and 20) and the 0015 (Refs. 21 and 22), as well as at low Reynolds numbers ($2 \times 10^5 \leq Re \leq 4 \times 10^5$) (Refs. 9 and 23). The effect of the 0015 slot discontinuity on stall was assessed by acquiring data with the slot open and with the slot taped over in a smooth manner, both with boundary-layer tripping at $x/c = 10\%$ only. The gentle stalling characteristics, as exemplified by the poststall variation of C_l and C_m (Fig. 2b), are virtually independent of the slot detail (as well as the trip location). This is probably because the slot is relatively small, $h/R = 5.5\%$, and does not modify the airfoil geometry sufficiently to affect its stalling characteristics. Note however, that the slot does affect transition and possibly even the transition mechanism resulting in the small $C_{l,\max}$ differences observed presently. Nevertheless, these data are consistent with the observation that, on thick airfoils, trailing-edge stall occurs irrespective of the transition mechanism.[12] Finally, note that $C_{l,\max}$ increases with tripping that is further aft, $x/c = 10\%$, because this results in a boundary layer that is less prone to separation.[12]

Additional differences in the nature of stall can be assessed by considering airfoil upper surface pressures (Figs. 3a–3f). Poststall instantaneous pressure coefficients over the interval $T \equiv tU/c = 120$ are presented in Figs. 3a (0012) and 3b (0015). The flow over the 0012 at $\alpha \leq \alpha_s + 3^\circ$ is characterized by intervals of partially attached and fully separated states, for example, $\alpha_s + 1$ deg shown in Fig. 3a. The transition from one state to another is relatively rapid, $T \approx 10$ and is comparable to time taken for separation from, or attachment to, a deflected flap.[1,14] Surface-mounted tufts across the airfoil span

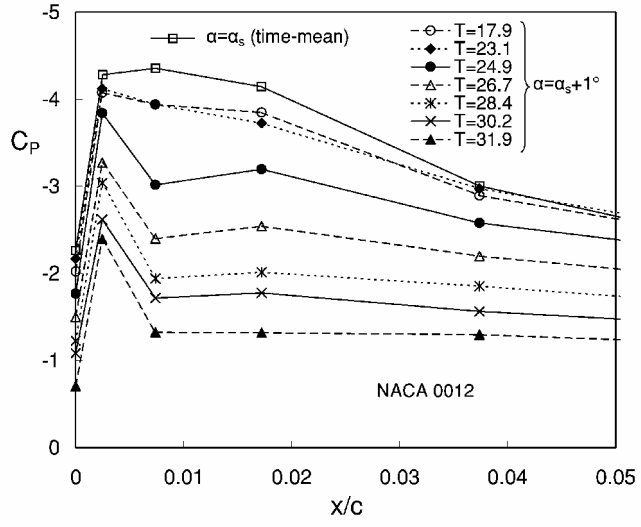

c)

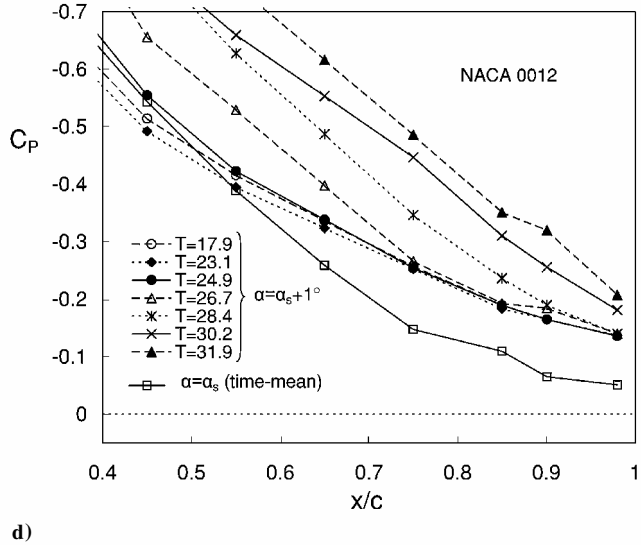

d)

Fig. 3c, d NACA 0012 upper-surface time-mean and instantaneous pressure in the c) leading- and d) trailing-edge regions during unsteady stall (c.f., Fig. 3a).

showed that both separation and attachment occurred in an essentially two-dimensional manner. Intervals of partially attached flow are characterized by a significant low pressure near the leading edge, $C_P \approx -4$, with an associated pressure recovery to $C_P \approx -0.15$ near the trailing edge, but these intervals are generally shorter than the fully separated intervals. Fourier analysis of pressure signals, as well as hot-wire measurements above the airfoil surface, indicated no regular "shedding-type" phenomenon. This lack of regular periodicity suggests that the phenomenon is somewhat different to that observed on certain low Reynolds number airfoils at the onset of stall.[24,25]

Figures 3c and 3d further illustrate respective upper surface leading-edge, $x/c < 0.05$, and aft-region, $x/c > 0.4$, instantaneous C_P during a typical dynamic separation at $\alpha = \alpha_s + 1^\circ$ during the interval $17.9 < T < 31.9$ (c.f., Fig. 3a). The time-mean C_P at incipient stall, $\alpha = \alpha_s$, is also plotted for comparative purposes in Figs. 3c and 3d. At $\alpha = \alpha_s$, the approximately constant C_P near the leading edge, followed by a steep pressure recovery,[26] indicates the existence of a separation bubble extending up to $x/c \approx 0.03$ (Fig. 3c). This is consistent with both high and low Reynolds number observations on the 0012 (Refs. 9 and 27). Examination of the trailing-edge region (Fig. 3d) shows that incipient separation is evident at $\alpha = \alpha_s$, and surface-mounted tufts confirmed these observations. Although the 0012 is generally known as a leading-edge staller, separation is observed to commence in the trailing-edge region under the present conditions.

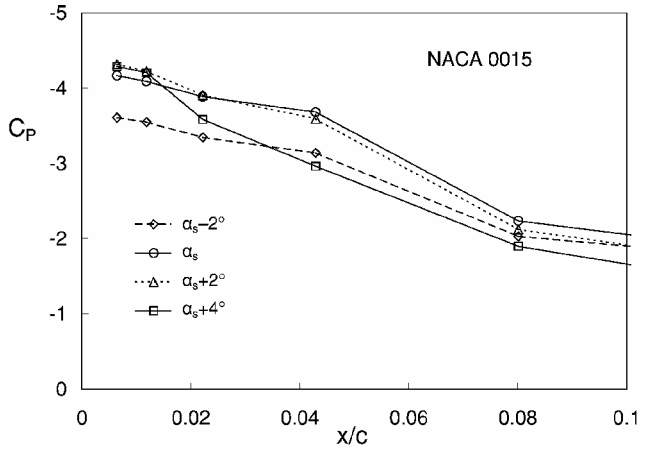

e)

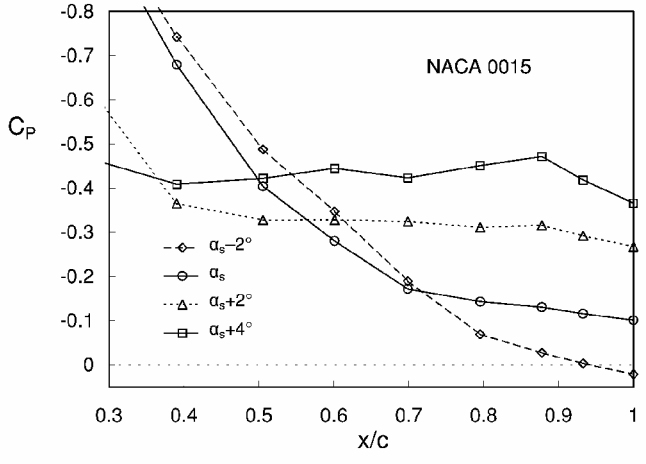

f)

Fig. 3e, f NACA 0015 upper surface time-mean pressures in the e) leading- and f) trailing-edge regions (c.f., Fig. 3b).

At $\alpha = \alpha_s + 1$ deg, the leading-edge bubble appears to "burst," as evident by the sharp pressure increase in the leading-edge region at $T = 24.9$ (Fig. 3c). Farther aft on the airfoil, $x/c > 0.5$, at the same instant, the pressures are unaffected (Fig. 3d). With increasing time, the leading-edge pressures increase rapidly, and the separated region is seen to progress farther downstream (Fig. 3d), reaching the trailing edge at $T \approx 28.4$. The bubble-bursting mechanism is presumed to be initiated by the high centrifugal acceleration of the flow as it negotiates the leading-edge radius.[11] Indeed, inviscid calculations (using a vortex panel method) show that the peak local acceleration (U_e^2/R) at α_s is twice as large on the 0012 as it is on the 0015. It is not clear, however, what triggers the quasi-periodic partial attachment and separation observed presently (Fig. 3a). Unlike the 0015, the 0012 leading-edge radius plays a crucial role in determining the nature of stall. Thus, the introduction of a 0012 slot at $x/c = 0$, similar to that of the 0015, would have altered its leading-edge radius and possibly its stalling characteristics.

McCroskey et al.[20] observed similar partial attachment and separation on a 0012 airfoil pitching in a quasi-steady manner beyond the static-stall angle at typical rotorcraft Reynolds numbers. (Comparison is not shown; see Ref. 13.) Furthermore, Currier and Fung[27] analyzed their data and determined that bubble bursting was the mechanism responsible for stall. They further ascertained that in subcritical cases the bubble-bursting mechanism is also responsible for dynamic stall, that is, when the airfoil is dynamically pitched beyond the static stall angle at rotorcraft reduced frequencies. Thus, control of this phenomenon, discussed in the next section, can be expected to have implications for the control of the dynamic stall vortex within the context of rotorcraft and dynamic stall.

The highly unsteady stalling mechanism of the 0012 (Fig. 3a) should be contrasted with that of the 0015 for $\alpha \geq \alpha_s$, for example, $\alpha = \alpha_s + 2$ deg shown in Fig. 3b. Moreover, the 0015 stall mechanism can be further assessed from the time-mean C_P distributions at representative incidence angles shown in Figs. 3e and 3f. The transition mechanism in the leading-edge region is not evident from Fig. 3e, but trailing-edge separation is evident at α_s (Fig. 3f), much like that associated with the 0012 at α_s (c.f., Fig. 3d). However, an increase in the incidence angle results in the separated region progressing upstream to $x/c \approx 0.5$ at $\alpha = \alpha_s + 2$ deg (c.f., Fig. 3b), but with no significant increase in the leading-edge pressure at $x/c < 0.1$ (Fig. 3e). A further increase in incidence angle moves the separation point farther forward on the airfoil (Fig. 3f), while the leading pressures at $x/c < 0.02$ remain effectively unchanged. In contrast to the dramatic 0012 bubble-bursting mechanism (Fig. 3a) turbulent fluctuations over the separated region of the 0015 are the main source of unsteadiness (Fig. 3b). The unsteady poststall lift and moment loads associated with the 0015 are up to 10 times smaller than those associated with the 0012. The impact of these different stalling characteristics on separation control is addressed in the next section.

Discussion of Control Results

Performance Enhancement

Separation control may be sensitive to the initial flow-state,[28] that is, whether control is applied to the post- or prestall scenario, and thus both were considered here. Post-stall control was applied [0012 ($\alpha_s + 2$ deg), and 0015 ($\alpha_s + 4$ deg)] for the frequency range $0 \leq F^+ \leq 6$ at $C_\mu = 0.2\%$ and $Re = 2 \times 10^5$, where both lift enhancement (Fig. 4a) and moment alleviation (Fig. 4b) were considered.

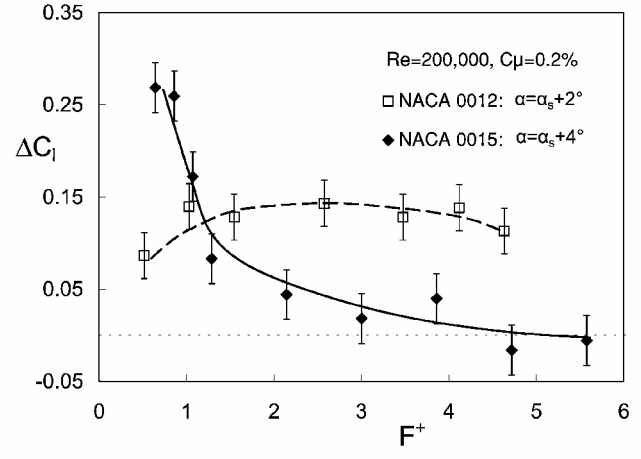

a)

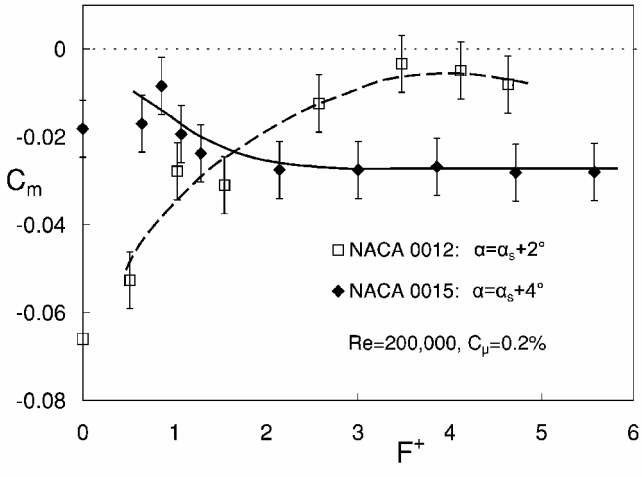

b)

Fig. 4 Effect of reduced excitation frequency (F^+) on poststall lift and moment for the NACA 0012 and 0015 airfoils under identical excitation conditions. Error bars represent maximum scatter; lines intended as a visual aid.

The 0015 produced maximum lift at $0.5 \leq F^+ \leq 1$, consistent with data taken previously over a smaller F^+ range,[2] and this interval increased slightly with higher excitation amplitudes (not shown, see Ref. 14.) Contrary to the 0015, the 0012 exhibited no well-defined optimum F^+ associated with lift enhancement; rather, the benefits were similar over the range $1.5 < F^+ < 4$. Despite this larger effective F^+ range, lift enhancement associated with the 0015 was nearly twice as much as that for the 0012. Data for both airfoils were found to be sensitive to initial F^+ and C_μ; thus the data presented here are averages of all data taken, and the maximum variation observed is indicated by the error bars.

In contrast to the 0012 ΔC_l data, C_m increases (approaches zero) with increasing F^+, and the most significant improvements are for $F^+ > 2$. Thus, at low-amplitude excitation, the higher frequencies are most effective reestablishing flow attachment on the airfoil. The reason for the apparent anomaly between ΔC_l (Fig. 4a) and C_m (Fig. 4b) data is elucidated by considering pressure distributions for relatively low, $F^+ = 0.51$, and high, $F^+ = 3.5$, frequencies (Fig. 5a). Here, the higher frequency is more effective in restoring the pressure recovery, even though both frequencies generate similar ΔC_l. For the 0015, poststall baseline C_m is far less severe (data at $F^+ = 0$) and thus excitation has a much smaller overall effect. Note, however, that the largest (closest to zero) moment coefficients coincide with the maximum ΔC_l due to enhanced attachment of the upper surface flow (Fig. 5b).

In the absence of curvature and transitional effects, with excitation at the separation location (controlled separation over a flap),[28] high F^+ (short wave-length) perturbations are amplified close to the excitation location, whereas low F^+ (long wave-length) perturbations are amplified farther downstream. Notwithstanding the effects of curvature and transition, the data shown in Figs. 4 and 5 are consistent with these observations, namely, that high F^+ excitation on the 0012 is most effective due to perturbation amplification close to the leading edge, whereas low F^+ excitation is most effective on the 0015 due to perturbation amplification farther downstream towards the trailing edge (shown subsequently).[14,28]

Control effectiveness on the 0012 was further assessed by initiating excitation in the prestall regime, $\alpha \leq \alpha_s$, and then increasing the incidence angle to $\alpha > \alpha_s$. An example of C_l and C_m vs α data for baseline and controlled, $F^+ = 1.5$, cases are presented in Figs. 6a and 6b for relatively low, $C_\mu = 0.09\%$, and relatively high, $C_\mu = 1.8\%$, excitation amplitudes. Low-amplitude excitation from the leading edge results in modest gains in $C_{l,\max}$, whereas the most significant effect is observed in the poststall regime; $\Delta C_l / C_l = 22\%$ at $\alpha = \alpha_s + 2$ deg. Increasing C_μ by a factor of 20 brought about significant overall lift enhancement, namely, $\Delta C_{l,\max} / C_{l,\max} = 25\%$ and $\Delta C_l / C_l = 60\%$ at $\alpha = \alpha_s + 3$ deg. Corresponding poststall negative C_m, concomitantly increased with increasing C_μ at a given α.

A summary of 0012 C_l data at $\alpha = \alpha_s + 3$ deg (Fig. 7a) for relatively low, $F^+ = 1.5$, and relatively high, $F^+ = 3.5$, reduced frequencies is considered, and these are further contrasted with steady blowing, $F^+ = 0$. For excitation at $C_\mu < 0.09\%$, the flow retained its unsteady character referred to earlier in Fig. 3a, whereas for $C_\mu \geq 0.09\%$, the flow stabilized and showed an increase in poststall lift (Fig. 7a). This should be contrasted with the 0015 (Fig. 7b), which showed significant lift increases at $C_\mu \approx 0.01\%$, that is, nine times less momentum input.[2] There are two possible, but not mutually exclusive, explanations for these observations. First, on the 0012, excitation must overcome the high centrifugal acceleration at the leading edge, which is appreciably less on the 0015. Second, the 45-deg slot at $x/c = 0.05$ is located downstream of the bubble reattachment location estimated at $x/c \approx 0.03$ from Fig. 3c. Thus, it may be less effective in controlling the bubble-bursting phenomenon described earlier.

For excitation at a given F^+ on the 0012, an increase in C_μ generally translates directly into an increase in C_l (Fig. 7a). However, this is not the case on the 0015 (Fig. 7b), which exhibits a peak in C_l at $C_\mu \approx 0.08\%$; thus, an increase in C_μ can degrade performance. Similar observations were made at different reduced frequencies in the range $1.1 \leq F^+ \leq 3.4$ (Ref. 7). On both airfoils, excitation is far superior to steady blowing, particularly for $C_\mu < 1\%$.

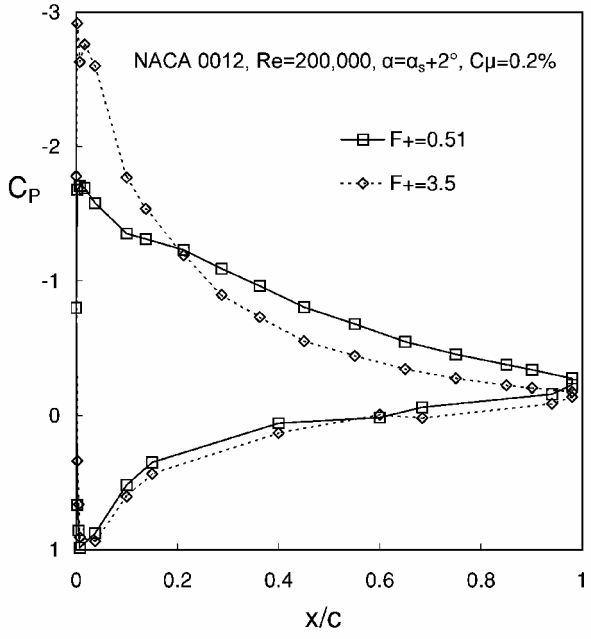

a)

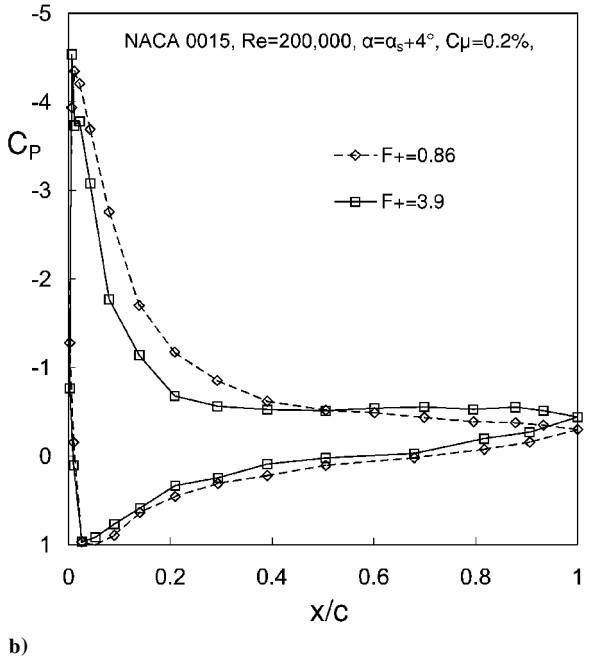

b)

Fig. 5 Effect of reduced frequency on the poststall pressure coefficient distribution.

Corresponding moment coefficients for the 0012 at various incidence angles, as a function of C_μ, are shown in Fig. 8. As in Figs. 6 and 7a, the flow was initially attached in all cases, and then α was increased beyond α_s. Consistent with the data of Fig. 4b, the combination of high F^+ and low C_μ is effective in increasing C_m at $\alpha_s + 2$ deg and to a somewhat lesser degree at $\alpha_s + 3$ deg. For $C_\mu > 0.2$, however, the lower frequency, $F^+ = 1.5$, is most effective for all incidence angles considered. Moreover, increases in C_μ consistently bring about increases in C_m. Note, however, that, at $\alpha_s + 5$ deg, approximately 10 times more C_μ is required to control moment stall than at $\alpha_s + 2$ deg, whereas excitation at $F^+ = 3.5$ is totally ineffective at $\alpha_s + 5$ deg irrespective of the magnitude of C_μ.

Figure 9 shows the 0012 leading- and trailing-edge C_P detail corresponding to the baseline and controlled cases in Fig. 6 for $\alpha_s - 1$ deg and $\alpha + 3$ deg. Before stall, $\alpha_s - 1$ deg, low-amplitude

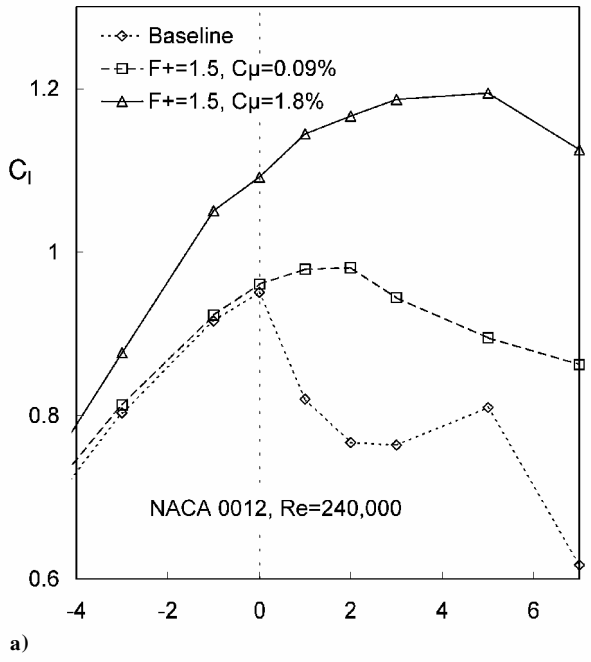

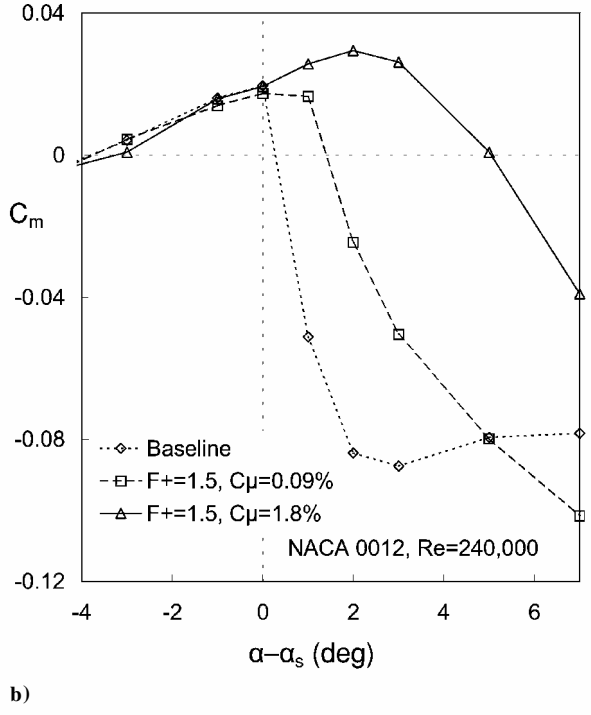

Fig. 6 Effect of low-amplitude and high-amplitude excitation on C_l and C_m.

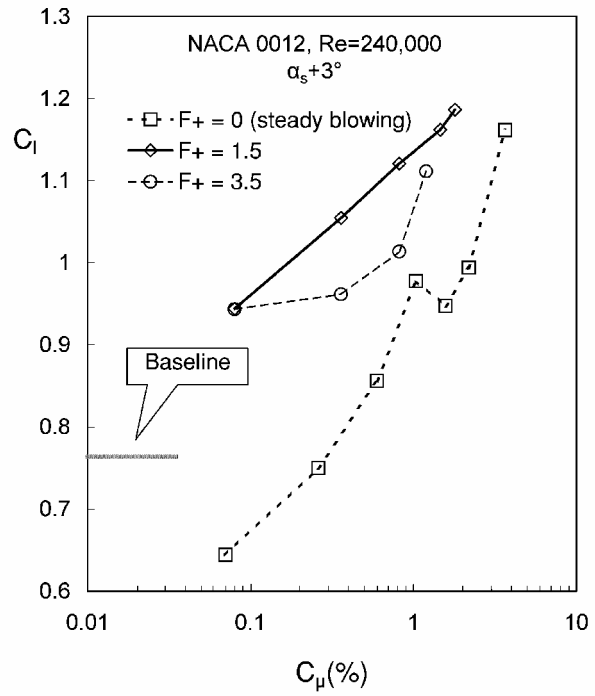

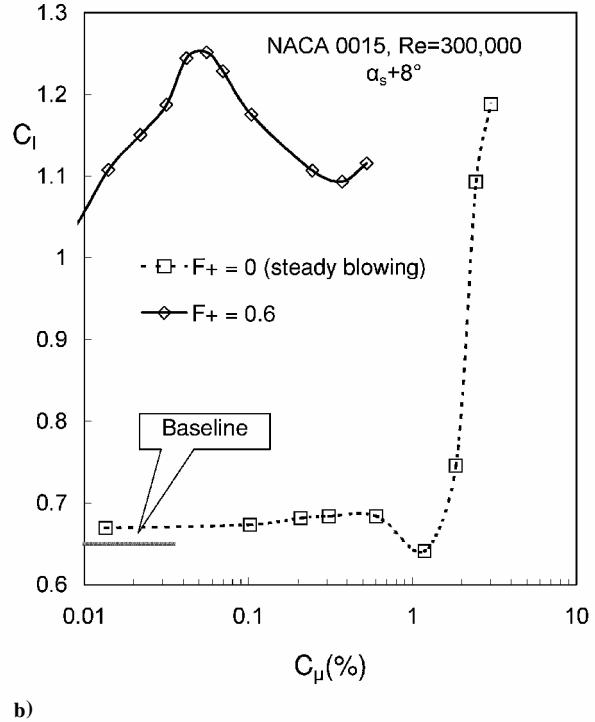

Fig. 7 Effect of momentum coefficient on poststall lift (0015 data from Ref. 2).

excitation, $C_\mu = 0.09\%$, has a negligible effect on the pressure distribution upstream of the slot, with a slightly deleterious effect at $x/c > 0.7$. However, at $C_\mu = 1.8\%$, excitation is effective for incidence angles lower than α_s, particularly at $\alpha_s - 1$ deg. This is apparently due to the modification, but not elimination of the leading-edge bubble, even though the excitation slot is downstream thereof. This also brings about improved boundary-layer attachment in the trailing-edge vicinity. At poststall angles, for example, $\alpha = \alpha_s + 3$ deg, shown in Fig. 9, the mechanism of lift enhancement is unchanged, that is, excitation downstream of the bubble prevents its bursting, even though separation has commenced in the trailing-edge region.

Turbulent boundary-layer spectra on the 0012 at $x/c = 30\%$, corresponding to $C_\mu = 0.09\%$ and 1.8% (Fig. 6), are shown for $\alpha = \alpha_s + 1$ deg in Fig. 10. At $C_\mu = 0.09\%$, the boundary layer shows conventional turbulent characteristics with no spectral peaks, and this indicates that perturbations introduced as a result of excitation decayed very close to the slot (c.f., Ref. 28). Furthermore phase-locked pressure fluctuations were not detectable above the background turbulent fluctuations. This result should be contrasted with that observed on the 0015, where phase-locked pressure fluctuations resulting from excitation at the airfoil leading edge ($F^+ = 0.6$ at $C_\mu = 0.1\%$) were still detectable at $x/c = 0.7$, even well into the poststall regime.[14,29] Amplitude decay over a short streamwise distance may also result because the excitation slot is located somewhat downstream of the separation bubble, and hence, the boundary layer is less receptive to amplification of the introduced perturbations.

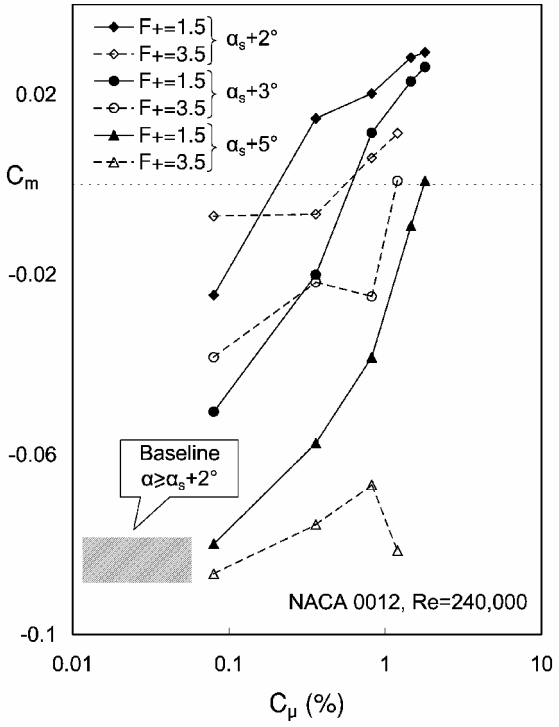

Fig. 8 Effect of momentum coefficient on NACA 0012 poststall moment coefficient.

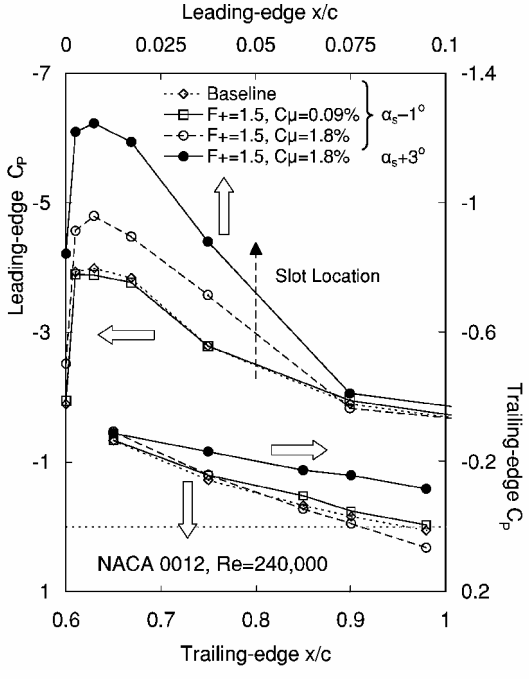

Fig. 9 Pressure distribution detail in the leading- and trailing-edge regions of the 0012 airfoil when subjected to low- and high-amplitude excitation at $F^+ = 1.5$.

In contrast to low-amplitude excitation, high-amplitude perturbations ($C_\mu = 1.8\%$) are clearly evident in the spectrum at the same location well downstream of the bubble. Also the large second harmonic, $f^+ = 3.0$, indicates that the growth of the perturbation is clearly non-linear, despite that the amplitude associated with the excitation frequency at the slot was an order of magnitude larger than its second harmonic (not shown). Large harmonics have been observed previously in the context of separation control over a Glauert–Goldschmied body (see Ref. 30). Presently, this observation may explain the apparent anomaly that high F^+ at low C_μ is effective in alleviating moment stall at low α (Figs. 4b and 8),

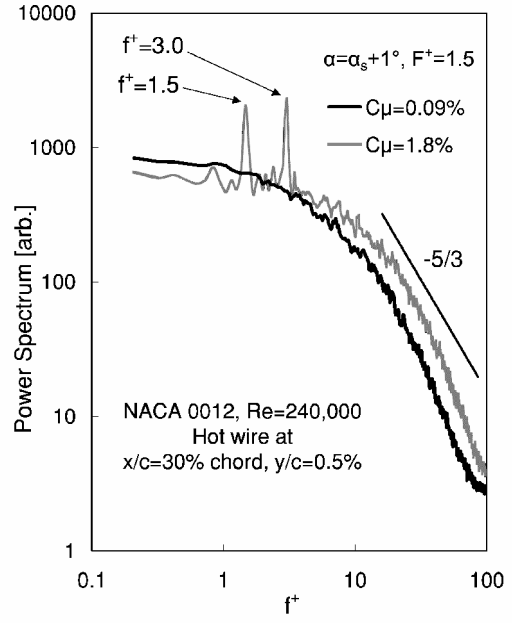

Fig. 10 Turbulent spectra measured in the boundary layer downstream of the excitation location.

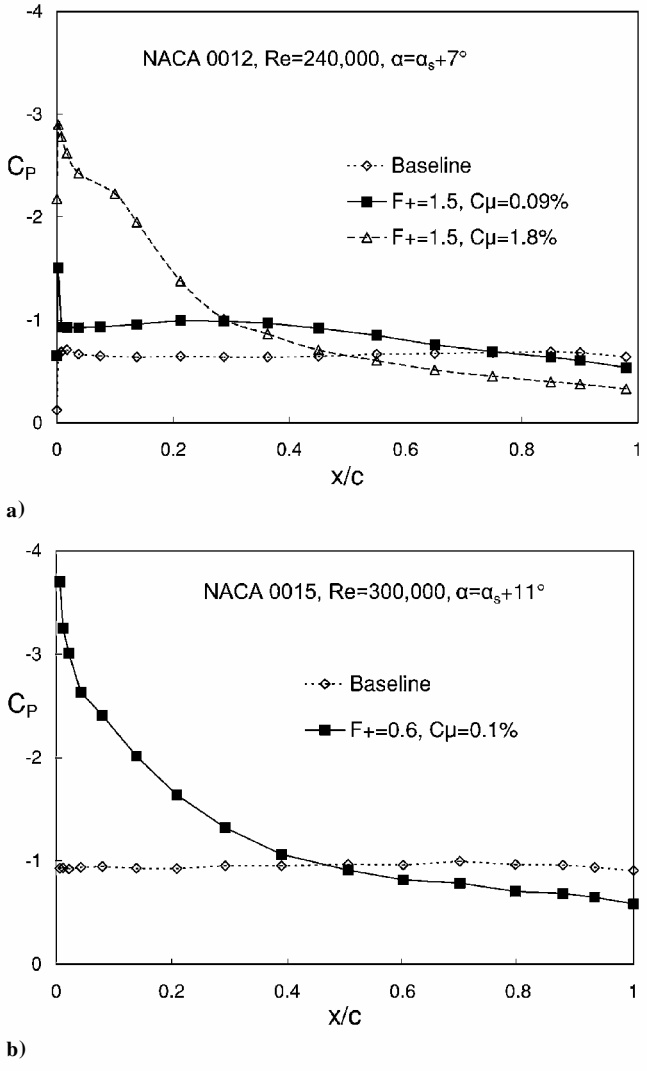

Fig. 11 Pressure distributions illustrating the effect of control on deep stall.

whereas low F^+ at high C_μ is effective at higher α (Fig. 8). Namely, high-amplitude excitation gives rise to higher harmonics, presently, $f^+ = 3.0$, which do not decay close to the slot and, hence, are also effective in controlling separation well downstream thereof. At higher excitation frequencies, for example, $F^+ = 3.5$, higher harmonics, $f^+ \geq 7.0$, presumably decay over a shorter streamwise distance and are, thus, less effective for separation control at high α.

Figures 11a and 11b show both airfoils well beyond α_s, such that fully separated flow pervades their upper surfaces (deep stall). On the 0012, low-amplitude excitation at all F^+ considered was ineffective in attaching the flow (data for $F^+ = 1.5$ shown in Fig. 11a), although partial attachment was possible for $C_\mu = 1.8\%$ at $F^+ = 1.5$. In contrast, low-amplitude excitation at $F^+ = 0.6$ on the 0015 brought about partial attachment on the upper surface (Fig. 11b). Unsteady surface pressure measurements, phase averaged over successive excitation cycles, showed that the perturbations amplified, reaching a maximum at $x/c \approx 0.15$, and then decayed gradually downstream (not shown, see Refs. 14 and 29). Similar observations were made at $F^+ = 1.1$, but further frequency increases degraded the effectiveness of control by confining its effect to the leading-edge region (not shown, see Refs. 14 and 29). Note finally that 20 times more C_μ was required to achieve a similar result on the 0012, thus further illustrating the impact of leading-edge radius on control effectiveness.

Control of Stall Unsteadiness

An important benefit associated with small amplitude excitation is the reduction in undesirable oscillatory flow associated with separation. Figures 12a and 12b show 0012 and 0015 poststall rms fluctuations C_l' and C_m', with and without control. Data were reduced from integration of the instantaneous surface pressures such as those shown in Figs. 3a and 3b. Baseline 0012 C_l' and C_m' are large close to the static stall angle, $\alpha - \alpha_s \leq 2$ deg, but are smaller at larger α as a consequence of the fully separated shear layer being farther from the airfoil surface. The largest effects of control are evident close to α_s, where C_l' and C_m' are reduced by factors of 5 and 10, respectively. Excitation increases the static stall angle by 2 and 3 deg at $F^+ = 1.5$ and 3.5, respectively, and this is reflected in the larger fluctuations evident at higher incidence angles. These can exceed the corresponding baseline data, but C_l' and C_m' maxima associated with excitation at both frequencies throughout this poststall incidence angle range are significantly smaller than those of the baseline maxima. At $\alpha - \alpha_s = 2$ deg, excitation at $F^+ = 3.5$ is most effective in controlling fluctuations, whereas for $\alpha - \alpha_s > 2$ deg, excitation at $F^+ = 1.5$ is superior, particularly for controlling C_m'.

On the 0015 baseline configuration, poststall C_l and C_m unsteadiness was small and, furthermore, the overall effect of excitation was negligible (c.f., Figs. 3a and 3b). It has been shown previously[2,29] that 0015 excitation has a small effect on C_l and C_m oscillations due to the cancellation effect of several vortices simultaneously present on the airfoil surface.

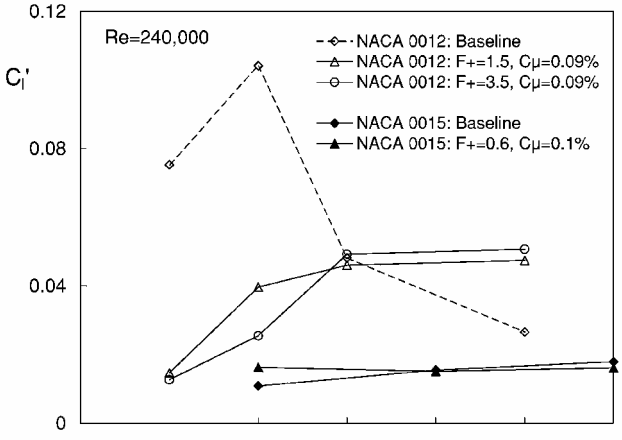

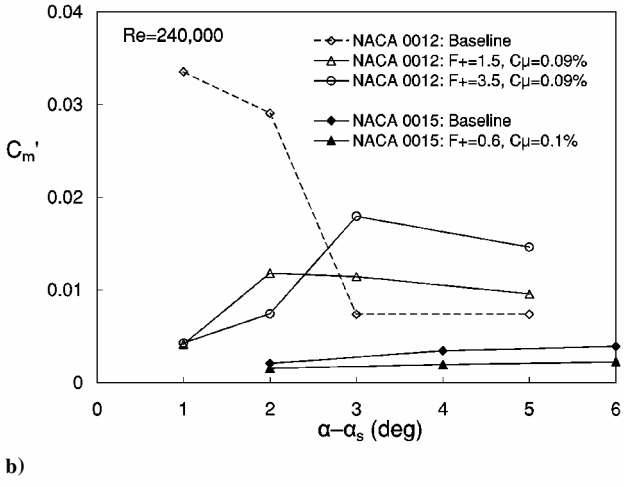

Fig. 12 Effect of low-amplitude excitation on poststall C_l and C_m unsteadiness.

Conclusions

The main conclusions regarding the nature of 0012 static stall and its control are summarized and the principal differences between the 0012 and 0015 airfoils follow.

1) Baseline 0012 stall was dominated by a bubble-bursting mechanism, which gave rise to alternating intervals of partial attachment and separation, but with no regular frequency. This was contrasted with the relatively gentle trailing-edge stall of the 0015.

2) The mechanism of 0012 separation control was identified as enhanced flow attachment downstream of the separation bubble without eliminating the bubble itself. The combination of high leading-edge curvature and excitation downstream of the bubble rendered the flow less receptive to excitation than the 0015 under similar conditions.

3) Relatively low amplitude excitation, (approximately $C_\mu < 0.2\%$, produced only modest lift increments over the reduced frequency range $0.5 < F^+ < 5$, with no clear optimum F^+. Moment coefficients, however, showed that low-amplitude lift generated at $F^+ < 1$ was inefficient. At higher amplitudes, approximately $C_\mu > 0.2\%$, excitation at $F^+ < 2$ was found to be superior. It was believed that the large harmonic content of the perturbations at the higher amplitudes was responsible for this apparent anomaly. In contrast, excitation on the 0015 at $0.5 < F^+ < 1$ was effective in increasing lift, but totally ineffective at $F^+ > 2$.

4) For a given excitation frequency, the 0012 required $C_\mu \sim \mathcal{O}$ (0.1%) to bring about increases in poststall lift and significant reductions in poststall unsteadiness. In contrast, 0015 had negligible poststall unsteadiness associated with it and required only $C_\mu \sim \mathcal{O}$ (0.01%) to produce meaningful lift enhancements.

Acknowledgments

This work was sponsored in part by a grant from the Research and Development Office of the Israel Ministry of Defense and is an assigned task of the U.S./Israel MOA on rotorcraft aeromechanics. The assistance of G. Hasdai is gratefully acknowledged.

References

[1] Greenblatt, D., and Wygnanski, I., "Control of Separation by Periodic Excitation," *Progress in Aerospace Sciences*, Volume 37, No. 7, 2000, pp. 487–545.

[2] Seifert, A., Darabi, A., and Wygnanski, I., "Delay of Airfoil Stall by Periodic Excitation," *Journal of Aircraft*, Vol. 33, No. 4, 1996, pp. 691–698.

[3] Naveh, T., Seifert, A., Tumin, A., and Wygnanski, I., "Sweep Effect on Parameters Governing Control of Separation by Periodic Excitation," *AIAA Journal*, Vol. 35, No. 3, 1998, pp. 510–512.

[4] Seifert, A., and Pack, L. G., "Oscillatory Control of Separation at High Reynolds Numbers," *AIAA Journal*, Vol. 37, No. 9, 1999, pp. 1062–1071.

[5] Seifert, A., and Pack, L. G., "Oscillatory Control of Shock-Induced Separation," *Journal of Aircraft*, Vol. 38, No. 3, 2001, pp. 464–472.

[6]Bachar, T., Wygnanski, I., and Ashpis, D., "Active Control of Separation in the Presence of High Freestream Turbulence," *Control of Turbulent Flows*, American Physical Society, Philadelphia, Nov. 1998, Abstract JK.01.

[7]Greenblatt, D., and Wygnanski, I., "Dynamic Stall Control by Periodic Excitation, Part 1: NACA 0015 Parametric Study," *Journal of Aircraft*, Vol. 38, No. 3, 2001, pp. 430–438.

[8]McCroskey, W. J., "A Critical Assessment of Wind Tunnel Results for the NACA 0012 Airfoil," NASA TM 100019, Oct. 1987.

[9]Park, Y. W., Lee, S. -G., Lee, D. -H., and Hong, S., "Stall Control with Local Surface Buzzing on a NACA 0012 Airfoil," *AIAA Journal*, Vol. 39, No. 7, 2001, pp. 1400–1402.

[10]Magill, J., Bachmann, M., Rixon, G., and McManus, K., "Dynamic Stall Control Using a Model-Based Observer," AIAA Paper 2001-0251, Jan. 2001.

[11]Stepniewski, W. Z., and Keys, C. N., *Rotary-Wing Aerodynamics*, Dover, New York, 1984, Chap. 6, pp. 310–312.

[12]Chang, P. K., *Control of Separation*, McGraw–Hill, New York, 1976, pp. 22–24.

[13]Greenblatt, D., and Wygnanski, I., "Effect of Leading-Edge Curvature on Separation Control: A Comparison of Two NACA Airfoils," AIAA Paper 2002-0411, Jan. 2002.

[14]Greenblatt, D., Darabi, A., Nishri, B., and Wygnanski, I., "Some Factors Affecting Stall Control with Particular Emphasis on Dynamic Stall," AIAA Paper 99-3504, June–July 1999.

[15]Piziali, R. A., "2-D and 3-D Oscillating Wing Aerodynamics for a Range of Angles of Attack Including Stall," NASA TM 4632, Sept. 1994.

[16]Bachar, T., "Generating Dynamically Controllable Oscillatory Fluid Flow," U.S. Patent 6,186,412, filed 13 Feb 2001.

[17]Liebeck, R. H., "Laminar Separation Bubbles and Airfoil Design at Low Reynolds Numbers," AIAA Paper 92-2735-CP, June 1992.

[18]Nagib, H., Kiedaisch, J., Greenblatt, D., Wygnanski, I., and Hassan, A., "Effective Flow Control for Rotorcraft Applications at Flight Mach Numbers," AIAA Paper 2001-2974, June 2001.

[19]Abbott, I. H., and von Doenhoff, A. E., *Theory of Wing Sections*, Dover, New York, 1959, pp. 462–463.

[20]McCroskey, W. J., McAlister, K. W., Carr, L. W., and Pucci, S. L., "An Experimental Study of Dynamic Stall on Advanced Airfoil Sections. Volume 2. Pressure and Force Data" NASA TM 84245, 1982.

[21]Pope, A., "The Forces and Moments over an NACA 0015 Airfoil," *Aero Digest*, Vol. 58, No. 4, 1949, pp. 76, 78, 100.

[22]Rice, M. S., *Handbook of Airfoil Sections for Light Aircraft*, Aviation Publications, Milwaukee, WI, 1971, p. 47.

[23]Dexin, H., and Weizhi, Z., "Aerodynamic Performance of 30 Types of Airfoil at High Angles of Attack," CARDC Low Speed Aerodynamics Inst., China Wind Energy Development Center, Mianyang, People's Republic of China, 1989, pp. 7–16 (in Chinese).

[24]Zaman, K. B. M. Q., McKinzie, D. J., and Rumsey, C. L. "A Natural Low-Frequency Oscillation of Flow over an Airfoil Near Stalling Conditions," *Journal of Fluid Mechanics*, Vol. 202, 1989, pp. 403–442.

[25]Broeren, A. P., and Bragg, M. B., "Flowfield Measurements over an Airfoil During Natural Low-Frequency Oscillations near Stall," *AIAA Journal*, Vol. 37, No. 1, 1999, pp. 130–132.

[26]Schmidt, G. S., and Mueller, T. J., "Analysis of Low Reynolds Number Separation Bubbles Using Semi-Empirical Methods," *AIAA Journal*, Vol. 27, No. 8, 1989, pp. 993–1001.

[27]Currier, J. M., and Fung, K. -Y., "Analysis of the Onset of Dynamic Stall," *AIAA Journal*, Vol. 30, No. 10, 1992, pp. 2469–2477.

[28]Nishri, B., and Wygnanski, I. "Effects of Periodic Excitation on Turbulent Separation from a Flap," *AIAA Journal*, Vol. 36, No. 4, 1998, pp. 547–556.

[29]Greenblatt, D., Nishri, B., Darabi, A., and Wygnanski, I., "Dynamic Stall Control by Periodic Excitation, Part 2: Mechanisms," *Journal of Aircraft*, Vol. 38, No. 3, 2001, pp. 439–447.

[30]Pack, L. G., and Seifert, A., "Dynamics of Active Separation Control at High Reynolds Numbers," AIAA Paper 2000-0409, Jan. 2000 (accepted for publication in the Royal Aeronautical Journal, England, 2003).